

Pharmacologic Activation of Integrated Stress Response Kinases Inhibits Pathologic Mitochondrial Fragmentation

Kelsey R. Baron^{1,7}, Samantha Oviedo^{1,2,7}, Sophia Krasny¹, Mashiat Zaman³, Rama Aldakhllallah¹, Prakhyat Mathur¹, Gerald Pfeffer⁴, Michael J. Bollong⁵, Timothy Shutt⁶, Danielle A. Grotjahn^{2,*}, R. Luke Wiseman^{1,*}

¹Department of Molecular and Cellular Biology, The Scripps Research Institute, La Jolla, CA 92037

²Department of Integrative Structural and Computation Biology, The Scripps Research Institute, La Jolla, CA 92037

³Department of Biochemistry and Molecular Biology, Cummings School of Medicine, University of Calgary, Calgary, Alberta, Canada

⁴Hotchkiss Brain Institute, Department of Clinical Neurosciences, Cumming School of Medicine, University of Calgary; Alberta Child Health Research Institute, Department of Medical Genetics, Cumming School of Medicine, University of Calgary

⁵Department of Chemistry, The Scripps Research Institute, La Jolla, CA 92037

⁶Departments of Medical Genetics and Biochemistry & Molecular Biology, Cumming School of Medicine, Hotchkiss Brain Institute, Snyder Institute for Chronic Diseases, Alberta Children's Hospital Research Institute, University of Calgary, Calgary, Alberta, Canada

⁷These authors contributed equally.

* Corresponding authors.

R. Luke Wiseman

Dept. of Molecular and Cellular Biology
The Scripps Research Institute
La Jolla, CA 92037
Email: wiseman@scripps.edu

Danielle A. Grotjahn

Dept. of Integrative Structural and Computational Biology
The Scripps Research Institute
La Jolla, CA 92037
Email: grotjahn@scripps.edu

SUMMARY

Excessive mitochondrial fragmentation is associated with the pathologic mitochondrial dysfunction implicated in the pathogenesis of etiologically-diverse diseases, including many neurodegenerative disorders. The integrated stress response (ISR) – comprising the four eIF2 α kinases PERK, GCN2, PKR, and HRI – is a prominent stress-responsive signaling pathway that regulates mitochondrial morphology and function in response to diverse types of pathologic insult. This suggests that pharmacologic, stress-independent activation of the ISR represents a potential strategy to mitigate pathologic mitochondrial fragmentation associated with human disease. Here, we show that pharmacologic, stress-independent activation of the ISR kinases HRI or GCN2 promotes adaptive mitochondrial elongation and prevents mitochondrial fragmentation induced by the calcium ionophore ionomycin. Further, we show that stress-independent activation of these ISR kinases reduces mitochondrial fragmentation and restores basal mitochondrial morphology in patient fibroblasts expressing the pathogenic D414V variant of the pro-fusion mitochondrial GTPase MFN2 associated with neurological dysfunctions including ataxia, optic atrophy, and sensorineural hearing loss. These results identify pharmacologic, stress-independent activation of ISR kinases as a potential strategy to prevent pathologic mitochondrial fragmentation induced by disease-relevant chemical and genetic insults, further motivating the pursuit of highly selective ISR kinase-activating compounds as a therapeutic strategy to mitigate mitochondrial dysfunction implicated in diverse human diseases.

INTRODUCTION

The integrated stress response (ISR) comprises four stress-regulated kinases – PERK, PKR, GCN2, and HRI – that selectively phosphorylate eIF2 α in response to diverse pathologic insults.^{1,2} The ISR has recently emerged as a prominent stress-responsive signaling pathway activated by different types of mitochondrial stress.³⁻⁵ Mitochondrial uncoupling or inhibition of ATP synthase activates the ISR through a mechanism involving the cytosolic accumulation and oligomerization of the mitochondrial protein DELE1, which binds to and activates the ISR kinase HRI.⁶⁻¹¹ Complex I inhibition can also activate the ISR downstream of the ISR kinase GCN2.¹² Further, CRISPRi-depletion of mitochondrial proteostasis factors preferentially activates the ISR over other stress-responsive signaling pathways.¹³ These results identify the ISR as an important stress-responsive signaling pathway activated in response to many different mitochondrial insults.

Consistent with its activation by mitochondrial stress, the ISR regulates many aspects of mitochondrial biology. ISR kinases are activated in response to stress through a conserved mechanism involving dimerization and autophosphorylation.^{1,2} Once activated, these kinases phosphorylate eIF2 α , resulting in both a transient attenuation of new protein synthesis and the activation of stress-responsive transcription factors such as ATF4.^{1,2} The ISR promotes adaptive remodeling of mitochondrial pathways through both transcriptional and translational signaling. For example, the activation of ATF4 downstream of phosphorylated eIF2 α transcriptionally regulates the expression of mitochondrial chaperones (e.g., the mitochondrial HSP70 *HSPA9*) and proteases (e.g., the AAA+ protease *LON*), increasing mitochondrial proteostasis capacity during stress.^{14,15} ISR-dependent translational attenuation also enhances mitochondrial proteostasis through the selective degradation of the core import subunit TIM17A, which slows mitochondrial protein import and reduces the load of newly-synthesized proteins entering mitochondria during stress.¹⁶ Apart from proteostasis, transcriptional and translational signaling induced by the activation of ISR kinases also regulates many other mitochondrial functions, including phospholipid synthesis, cristae organization, and electron transport chain activity.¹⁷⁻²¹

Intriguingly, the morphology of mitochondria is also regulated by ISR signaling. Mitochondrial morphology is dictated by the relative activities of pro-fission and pro-fusion GTPases localized to the outer and inner mitochondrial membranes (OMM and IMM, respectively).^{22,23} These include the pro-fusion GTPases MFN1 and MFN2 and the pro-fission GTPase DRP1, all localized to the OMM. Previous results showed that ER stress promotes adaptive mitochondrial elongation downstream of the PERK arm of the ISR through a mechanism

involving the accumulation of the phospholipid phosphatidic acid on the OMM where it inhibits the pro-fission GTPase DRP1.^{20,21,24} This PERK-dependent increase of mitochondrial elongation functions to protect mitochondria during ER stress through multiple mechanisms, including enhanced regulation of respiratory chain activity, suppression of mitochondrial fragmentation, and reductions in the turnover of mitochondria by mitophagy.^{20,21} Apart from PERK, stress-independent, pharmacologic activation of the alternative ISR kinase GCN2 also promotes adaptive mitochondrial elongation.²⁴ This indicates that mitochondrial elongation may be a protective mechanism that can be pharmacologically accessed by activating multiple different ISR kinases.

Excessive mitochondrial fragmentation is a pathologic hallmark of numerous human diseases, including several neurodegenerative disorders.^{22,25-28} Fragmented mitochondria are often associated with mitochondrial dysfunctions including impaired respiratory chain activity and dysregulation of mitophagy.^{22,25-30} Thus, pathologic increases in mitochondrial fragmentation are linked to many mitochondrial dysfunctions implicated in human disease. Consistent with this observation, interventions that prevent mitochondrial fragmentation have been shown to correct pathologic mitochondrial dysfunction in models of many different diseases.^{31,32} Notably, genetic or pharmacologic inhibition of the pro-fission GTPase DRP1 blocks pathologic mitochondrial fragmentation and subsequent mitochondrial dysfunction in cellular and *in vivo* models of diverse neurodegenerative diseases, including Charcot-Marie-Tooth Type 2A and Type 2B, spastic paraplegia, optic atrophy, Huntington's disease, Amyotrophic Lateral Sclerosis, and Alzheimer's disease.³³⁻⁴⁴

The ability of ISR activation to promote mitochondrial elongation suggests that pharmacologic, stress-independent activation of ISR kinases could mitigate the pathologic mitochondrial fragmentation implicated in etiologically diverse human diseases. To test this idea, we probed the potential for pharmacologic activation of different ISR kinases to reduce mitochondrial fragmentation induced by disease-relevant chemical and genetic insults. Previous work identified the small molecule halofuginone as a potent activator of the ISR kinase GCN2 that promotes ISR-dependent, adaptive mitochondrial elongation.^{45,46} However, few other compounds were available that selectively activated other ISR kinases and were suitable for probing mitochondrial adaptation induced by ISR kinase activation.²⁴ Here, we used a small molecule screening platform to identify two nucleoside mimetic compounds, 0357 and 3610, that preferentially activate the ISR downstream of the ISR kinase HRI. Using these compounds, we demonstrate that pharmacologic activation of HRI also promotes adaptive, ISR-dependent mitochondrial elongation. We go on to show that pharmacologic activation of ISR kinases with these

compounds prevents DRP1-mediated mitochondrial fragmentation induced by the calcium ionophore ionomycin.^{47,48} Further, we show that compound-dependent activation of ISR kinases reduces the population of fragmented mitochondria and rescues basal mitochondrial network morphology in patient fibroblasts expressing the D414V variant of the pro-fusion GTPase MFN2 associated with a complex clinical phenotype including ataxia, optic atrophy and sensorineural hearing loss.⁴⁹ These results demonstrate the potential for pharmacologic, stress-independent activation of different ISR kinases to prevent pathologic mitochondrial fragmentation in disease-relevant models. Moreover, our work further motivates the continued development of highly selective activators of ISR kinases as a potential therapeutic strategy to mitigate the pathologic mitochondrial dysfunction implicated in etiologically diverse human diseases.

RESULTS

The nucleoside mimetic compounds 0357 and 3610 preferentially activate the ISR downstream of HRI

The small molecule halofuginone activates the ISR kinase GCN2 and induces ISR-dependent mitochondrial elongation.^{45,46} However, few other compounds are available that selectively activate other ISR kinases through mechanisms that allow for ISR-dependent mitochondrial remodeling.⁴⁶ For example, BtdCPU activates the ISR kinase HRI through a mechanism involving mitochondrial uncoupling, precluding its use for probing ISR-dependent protection of mitochondria.⁴⁶ To address this limitation and define the potential for pharmacologic activation of other ISR kinases to promote adaptive mitochondrial elongation, we established and implemented a screening platform to identify compounds that activated ISR signaling downstream of alternative ISR kinases (**Fig. 1A**). In this screen, we used the ATF4-FLuc translational reporter of the ISR (**Fig. S1A**).¹¹ We confirmed that ISR activating stressors including the ER stressor thapsigargin (Tg) and the ATP synthase inhibitor oligomycin A (OA) robustly activated this reporter (**Fig. S1B**). We then used this reporter to screen the ~3k nucleoside mimetic analog compound library (10 µM) and monitored ATF4-FLuc activity 8 h after treatment. Our primary screen identified 34 hit compounds that activated the ATF4-FLuc reporter with a robust Z-score >3-fold. We then removed highly reactive compounds and pan-assay interference compounds (PAINS), which reduced the number of hits to 9 (**Fig. 1B**). These compounds were re-purchased and then tested in dose response for ATF4-FLuc activation (**Fig. S1C**). This identified compounds 0357 and 3610 as the compounds that most efficaciously activated the ATF4-FLuc reporter, albeit with low potency ($EC_{50} > 10 \mu M$). We confirmed that co-

treatment with the highly selective ISR inhibitor ISRIB^{50,51} blocked ATF4-FLuc activation induced by these compounds, confirming this activation can be attributed to the ISR (**Fig. 1C,D**). Further, we used qPCR to show that treatment with 0357 or 3610 increased expression of the ISR target genes ASNS and CHAC1 in HEK293 and MEF cells (**Fig. S1D,E**).^{52,53} Importantly, these compounds did not activate luciferase reporters of other stress-responsive signaling pathway such as the unfolded protein response (UPR; XBP1-RLuc)^{54,55}, the heat shock response (HSR; HSE-FLuc)⁵⁶, or the oxidative stress response (OSR; ARE-FLuc)⁵⁷ (**Fig. 1E,F**). Further, treatment with these compounds did not induce expression of the UPR target gene *BiP*, the HSR target gene *HSPA1A*, or the OSR target gene *NQO1* in HEK293 cells (**Fig. S1F**). These results indicate compounds 0357 and 3610 preferentially activate the ISR, as compared to other stress responsive signaling pathways.

Next, we sought to identify the specific ISR kinases responsible for ISR activation induced by these two nucleoside mimetics. We monitored the compound-dependent activation of an ATF4-mAPPLE fluorescent reporter stably expressed in HEK293 cells CRISPRi-depleted of each individual ISR kinase (**Fig. S1A**).^{8,46} We previously used this assay to confirm that halofuginone activates the ISR downstream of GCN2 and BtdCPU activates the ISR downstream of HRI.⁴⁶ Treatment with either 0357 or 3610 activates the ATF4-mAPPLE reporter in control cells (**Fig. 1G,H**). CRISPRi-depletion of *HRI*, but no other ISR kinase, blocked ATF4-FLuc activation induced by these two compounds. This finding indicates that these compounds activate the ISR downstream of HRI. Collectively, these results identify 0357 and 3610 as nucleoside mimetic compounds that preferentially activate the ISR through a mechanism involving the ISR kinase HRI.

Pharmacologic HRI activation promotes mitochondrial elongation.

Halofuginone-dependent activation of GCN2 promotes adaptive mitochondrial elongation.⁴⁶ However, it is currently unclear if pharmacologic, stress-independent activation of other ISR kinases can similarly induce mitochondrial elongation. Here, we tested the ability of our HRI-activating compounds 0357 and 3610 to induce mitochondrial elongation downstream of the ISR. Previously, ISR-dependent mitochondrial elongation was quantified by manually classifying cells as containing fragmented, tubular, or elongated networks.^{20,21} However, since 0357 and 3610 activate ISR signaling to lower levels than that observed for other compounds (e.g., halofuginone), we posited that these compounds may induce more modest mitochondrial elongation that may be difficult to quantify using this manual approach. To address this, we implemented an automated image

analysis pipeline using Imaris software to quantify mitochondrial elongation in MEF cells stably expressing mitochondrial-targeted GFP (^{mt}GFP) treated with our compounds (**Fig. S2A**).⁵⁸ We collected Z-stack confocal images of ^{mt}GFP-expressing MEF cells (MEF^{mtGFP}) and processed images using a deconvolution filter in FIJI to reduce the background and enhance the fluorescent signal. We used the “Surfaces” module on Imaris to generate three-dimensional (3D) segmentation models of mitochondria visible in the deconvolved Z-stacks. Using the surfaces module, we quantified parameters defining mitochondrial shape, including bounding box length, sphericity, and ellipsoid principal axis length (**Fig. S2A**). Treatment with conditions that induce mitochondrial elongation, such as the ER stressor thapsigargin (Tg) and the GCN2 activator halofuginone (HF), increased bounding box and ellipsoid principal axis length, while reducing sphericity (**Fig. 2A-D, Fig. S2B-D**) – all changes consistent with increases in mitochondrial length. In contrast, treatment with conditions that promote mitochondrial fragmentation, such as the mitochondrial uncouplers BtdCPU and CCCP (both compounds that activate HRI)^{6,46}, reduced bounding box length and ellipsoid principal axis length, while increasing sphericity (**Fig. 2A-D, Fig. S2B-D**) – all changes consistent with increased mitochondrial fragmentation.

We next applied this approach to define the impact of pharmacologic, stress-independent HRI activation on mitochondrial morphology. Treatment with either 0357 or 3610 for 6 h increased both the bounding box and ellipsoid principal axis length, while decreasing mitochondrial sphericity (**Fig. 2A-D**). This result indicates that both these compounds induced mitochondrial elongation. Co-treatment with the selective ISR inhibitor ISRB blocked these changes in mitochondria shape, indicating that these compounds induce mitochondrial elongation through an ISR-dependent mechanism (**Fig. 2E-H**). ISRB co-treatment also blocked mitochondrial elongation induced by the ER stressor thapsigargin (Tg) and the GCN2 activator halofuginone (HF), as predicted.^{20,46} These results indicate that, like halofuginone, pharmacologic activation of HRI with compounds 0357 and 3610 induce adaptive, ISR-dependent mitochondrial elongation. Further, these suggest that the pharmacologic activation of different ISR kinases can induce protective elongation of mitochondria in the absence of cellular stress.

Pharmacologic ISR activation suppresses ionomycin-induced mitochondrial fragmentation.

The ability for pharmacologic activation of GCN2 or HRI to induce adaptive mitochondrial elongation suggests that enhancing signaling through these kinases may suppress mitochondrial fragmentation induced by pathologic insults such as calcium dysregulation.⁵⁹⁻⁶² Treatment with the calcium ionophore, ionomycin, induces rapid,

DRP1-dependent mitochondrial fragmentation in cell culture models.^{47,48} We pre-treated MEF^{mtGFP} cells for 6 h with the GCN2 activator halofuginone or our two HRI activating compounds (0357 and 3610) and subsequently challenged these cells with ionomycin. We then monitored mitochondrial morphology over a 15-minute timecourse. As expected, ionomycin rapidly increased the accumulation of fragmented mitochondria in these cells, evidenced by reductions in both bounding box and ellipsoid principal axis length and increases of organelle sphericity (**Fig. S3A-D**). Pre-treatment with the ER stressor thapsigargin, which promotes stress-induced mitochondrial elongation downstream of the PERK ISR kinase, reduced the accumulation of fragmented mitochondria in ionomycin-treated cells (**Fig. 3A-D**), as previously reported.²¹ Intriguingly, treatment with halofuginone, 0357, or 3610 also reduced the accumulation of fragmented mitochondria in ionomycin-treated cells. Instead, mitochondria in cells pretreated with these ISR kinase activators and challenged with ionomycin demonstrated mitochondrial lengths and sphericity similar to that observed in vehicle-treated MEF^{mtGFP} cells (**Fig. 3A-D**). These results indicate that pharmacologic, stress-independent activation of different ISR kinases can suppress the accumulation of fragmented mitochondria following ionomycin-induced calcium dysregulation.

Stress-independent, pharmacologic activation of ISR kinases restores basal mitochondrial morphology in patient fibroblasts expressing disease-associated MFN2^{D414V}.

Over 150 pathogenic variants in the pro-fusion GTPase MFN2 are causatively associated with the autosomal dominant peripheral neuropathy Charcot-Marie-Tooth Type 2A.⁶³⁻⁶⁵ While these pathogenic variants can impact diverse aspects of mitochondrial biology⁶⁴, many, including D414V, lead to increases in mitochondrial fragmentation.^{49,63-65} This can be attributed to reduced activity of MFN2-dependent fusion associated with these variants and a subsequent relative increase of DRP1-dependent mitochondrial fission. We predicted that pharmacologic, stress-independent activation of ISR kinases could rescue mitochondrial network morphology in patient fibroblasts expressing the disease-associated MFN2 variant D414V (MFN2^{D414V}). To test this, we treated wild-type human fibroblasts and patient fibroblasts expressing MFN2^{D414V} with halofuginone or our two HRI activating compounds 0357 and 3610 and monitored mitochondrial network morphology by staining with MitoTracker. As reported previously, MFN2^{D414V}-expressing fibroblasts showed shorter, more fragmented mitochondrial networks, as compared to control fibroblasts, reflected by reductions in both bounding box and ellipsoid principle axis lengths and increased sphericity (**Fig. 4A, S4A-C**).⁴⁹ Treatment with halofuginone, 0357,

or 3610 increased mitochondrial length in control fibroblasts (**Fig. 4A-D**). All these changes were inhibited by co-treatment with ISRIB, confirming these effects can be attributed to ISR activation. Intriguingly, treatment with all three compounds also increased mitochondrial length and reduced sphericity in MFN2^{D414V}-expressing patient fibroblasts to levels similar to those observed in control fibroblasts, with halofuginone showing the largest effect (**Fig. 4A,F-H**). Again, this increase in mitochondrial elongation was reversed by co-treatment with ISRIB. These results show that pharmacologic activation of different ISR kinases can rescue basal mitochondrial morphology in patient fibroblasts expressing the disease-associated MFN2^{D414V} variant that causes dysregulation in various neurological functions including ataxia, optic atrophy, and sensorineural hearing loss.

DISCUSSION

Here, we show that pharmacologic, stress-independent activation of different ISR kinases can prevent mitochondrial fragmentation induced by disease-relevant chemical or genetic insults. We identify two nucleoside mimetic compounds that preferentially activate the ISR downstream of the ISR kinase HRI. We demonstrate that these two HRI activators promote adaptive, ISR-dependent mitochondrial elongation. Further, we show that treatment with these HRI-activating compounds or the GCN2 activator halofuginone prevents the accumulation of fragmented mitochondria induced by Ca²⁺ dysregulation and rescues mitochondrial network morphology in patient fibroblasts expressing the disease-associated, pathogenic D414V variant of MFN2. Collectively, these results demonstrate that pharmacologic, stress-independent activation of different ISR kinases can mitigate pathologic mitochondrial fragmentation induced by diverse disease-associated pathologic insults.

Mitochondrial fragmentation is often induced through a mechanism involving stress-dependent increases in the activity of the pro-fission GTPase DRP1.^{22,29} This has motivated efforts to identify pharmacologic inhibitors of DRP1 to prevent mitochondrial fragmentation and subsequent organelle dysfunction associated with human disease.^{32,39,66} Activation of the ISR kinase PERK during ER stress promotes mitochondrial elongation through a mechanism involving inhibition of DRP1.²¹ This suggested that pharmacologic, stress-independent activation of other ISR kinases could also potentially inhibit DRP1 and block pathologic mitochondrial dysfunction induced by increased DRP1 activity. Consistent with this idea, we show that pharmacologic activation of the ISR using both GCN2 and HRI activating compounds blocks the accumulation of fragmented mitochondria in ionomycin-treated cells – a condition that promotes mitochondrial fragmentation through increased DRP1-dependent

fission.^{47,48} These results support a model whereby stress-independent, pharmacologic activation of different ISR kinases promotes organelle elongation by inhibiting DRP1 and suggests that pharmacologic activation of ISR kinases can be broadly applied to quell mitochondrial fragmentation in the myriad diseases associated with overactive DRP1.

Pathogenic variants in mitochondrial-targeted proteins are causatively associated with the onset and pathogenesis of numerous neurodegenerative disorders, including Charcot-Marie-Tooth (CMT), spinocerebellar ataxia (SCA), and spastic paraplegia.^{22,25,67-70} In many of these diseases, mitochondrial fragmentation is linked to pathologic mitochondrial dysfunctions, such as reduced respiratory chain activity, decreased mtDNA, and increased apoptotic signaling. Intriguingly, pharmacologic or genetic inhibition of mitochondrial fragmentation mitigates cellular and mitochondrial pathologies associated with many of these diseases, highlighting the critical link between mitochondrial fragmentation and disease pathogenesis.^{34-36,44} Herein, we show that pharmacologic, stress-independent activation of the ISR mitigates mitochondrial fragmentation in patient fibroblasts homozygous for the disease-associated D414V MFN2 variant. This finding highlights the potential for pharmacologic ISR activation to restore basal mitochondrial network morphology in cells expressing pathogenic MFN2 variants, although further study is necessary to determine the impact of ISR activation in cells from heterozygous patients expressing pathogenic MFN2 variants associated with CMT2A, the most common clinical phenotype associated with this disease. Regardless, our results are of substantial interest because over 70% of cases of axonal CMT are associated with pathogenic MFN2 variants, and to date, no disease-modifying therapies are available for any genetic subtype of CMT.^{71,72} Apart from MFN2 variants, our results also highlight the potential for pharmacologic ISR kinase activation to broadly mitigate pathologic mitochondrial fragmentation associated with the expression of disease-related, pathogenic variants of other mitochondrial proteins, which we are continuing to explore.

Apart from morphology, ISR signaling also promotes adaptive remodeling of many other aspects of mitochondrial biology, including proteostasis, electron transport chain activity, phospholipid synthesis, and apoptotic signaling.¹⁴⁻²¹ While we specifically focus on defining the potential for pharmacologic activation of ISR kinases to rescue mitochondrial morphology in disease models, the potential of ISR activation to promote adaptive remodeling of other mitochondrial functions suggests that pharmacologic activators of ISR kinases could more broadly influence cellular and mitochondrial biology in disease states through the adaptive remodeling of these other pathways. For example, we previously showed that halofuginone-dependent GCN2

activation restored cellular ER stress sensitivity and mitochondrial electron transport chain activity in cells deficient in the alternative ISR kinase PERK⁴⁶ – a model of neurodegenerative diseases associated with reduced PERK activity such as PSP and AD.^{73,74} Compounds that activate other ISR kinases are similarly predicted to promote the direct remodeling of mitochondrial pathways to influence these and other functions. Thus, as we, and others, continue defining the impact of pharmacologic ISR kinase activation on mitochondrial function, we predict to continue revealing new ways in which activation of ISR kinases directly regulates many other aspects of mitochondrial function disrupted in human disease.

Several different compounds have previously been reported to activate specific ISR kinases.^{46,75-80} However, the potential for many of these compounds to mitigate mitochondrial dysfunction in human disease is limited by factors including lack of selectivity for the ISR or a specific ISR kinase, off-target activities, or low therapeutic windows.⁴⁶ For example, the HRI activator BtdCPU activates the ISR through a mechanism involving mitochondrial uncoupling and subsequent mitochondrial fragmentation.⁴⁶ Here, we identify two nucleoside mimetic compounds that activate the ISR downstream of HRI and show selectivity for the ISR relative to other stress-responsive signaling pathways, providing new tools to probe mitochondrial remodeling induced by ISR kinase activation. However, the low potency of these compounds limits their translational potential to mitigate mitochondrial dysfunction in disease, necessitating the identification of new, highly-selective ISR kinase activating compounds. As we and others continue identifying next-generation ISR kinase activators with improved translational potential, it will be important to optimize the pharmacokinetics (PK) and pharmacodynamic (PD) profiles of these compounds to selectively enhance adaptive, protective ISR signaling in disease-relevant tissues, independent of maladaptive ISR signaling often associated with chronic, stress-dependent activation of this pathway.^{1,2} As described previously for activators the IRE1 arm of the UPR, such improvements can be achieved by defining optimized compound properties and dosing regimens to control the timing and extent of pathway activity.⁸¹ Thus, as we and others continue pursuing pharmacologic ISR kinase activation as a strategy to target mitochondrial dysfunction in disease, we anticipate that we will continue to learn more about the central role for this pathway in adapting mitochondria during stress and establish pharmacologic ISR kinase activation as a viable approach to treat mitochondrial dysfunction associated with etiologically-diverse diseases.

MATERIALS AND METHODS

Mammalian Cell Culture

HEK293 cells (purchased from ATCC), HEK293 cells stably expressing XBP1-RLuc^{54,55}, HEK293 cells stably expressing HSE-FLuc, HEK293 cells stably expressing ATF4-mAPPLE (a kind gift from Martin Kampmann's lab)¹¹ and CRISPRi-depleted of individual ISR kinases (*HRI*, *PKR*, *PERK*, *GCN2*; a kind gift from Martin Kampmann's lab at UCSF)⁸, and MEF^{mtGFP} (a kind gift from Peter Schultz)⁵⁸ were all cultured at 37°C and 5% CO₂ in DMEM (Corning-Cellgro) supplemented with 10% fetal bovine serum (FBS, Gibco), 2 mM L-glutamine (Gibco), 100 U/mL penicillin, and 100 mg/mL streptomycin (Gibco).

Primary fibroblast cells were isolated from partial thickness skin biopsy, as previously described^{49,82}, from a patient who provided written informed consent for research studies using human tissues (University of Calgary Conjoint Research Ethics Board REB17-0850). Cells were cultured in Medium Essential Media (11095080, Gibco), supplemented with 10% Fetal Bovine Serum (12483020, Gibco). Cells were maintained at 37 °C and 5% CO₂. Clinical information regarding this participant was previously reported and included ataxia, optic atrophy, and sensorineural hearing loss.⁴⁹ Exome sequencing in this participant identified a homozygous c.1241A>T variant in *MFN2* (predicted to cause p.(Asp414Val)) and no other pathogenic variants.

Compounds and Reagents

Compound used in this study were purchased from the following sources: thapsigargin (Tg; Cat# 50-464-294 Fisher Scientific), ISRIB (Cat # SML0843, Sigma), CCCP (Cat #C2759,Sigma), BtdCPU (Cat #32-489-210MG, Fisher), halofuginone (Cat #50-576-3001, Sigma), and oligomycin A (S1478, Selleck). The nucleoside mimetic library was purchased from Chem Div. Hit compounds were repurchased from Chem Div.

Measurements of ISR activation in ATF4-reporter cell lines

HEK293 cells stably expressing the ATF4-FLuc, HSE-Fluc, or the ARE-Fluc reporter were seeded at a density of 15,000 cells per well in 384-well white plates with clear bottoms (Greiner). The following day, cells were treated with the indicated compound in triplicate at the indicated concentration for 8h. After treatment, an equal volume of Promega Bright-Glo substrate (Promega) was added to the wells and allowed to incubate at room temperature for 10 minutes. Luminescence was then measured using an Infinite F200 PRO plate reader (Tecan) with an integration time of 1000 ms. This assay was used to both screen the nucleoside mimetic library in triplicate and

monitor the activity of hit compounds. HEK293 cells expressing the XBP1-RLuc reporter were tested using an analogous approach to that described above, monitoring RLuc activity using Renilla-Glo reagent (Promega), as previously described.⁵⁴

HEK293 cells stably expressing the ATF4-mApple reporter and CRISPRi-depleted of specific ISR kinases were seeded at a density of 300,000 cells per well in 6-well TC-treated flat bottom plates (Genesee Scientific). Cells were treated the next day for 16 h with compound at the indicated concentration. Cells were then washed twice with phosphate-buffered saline (PBS) and dissociated using TrypLE Express (ThermoFisher). Cells were then resuspended in PBS and 5% FBS to neutralize the enzymatic reaction. Flow cytometry was performed on a Bio-Rad ZE5 Cell Analyzer monitoring mAPPLE fluorescence (568/592 nm) using the 561 nm green-yellow laser in combination with the 577/15 filter. Analysis was performed using FlowJoTM Software (BD Biosciences).

Quantitative Polymerase Chain Reaction (qPCR)

The relative mRNA expression of target genes was measured using quantitative RT-PCR. Cells were treated as indicated and then washed with phosphate-buffered saline (PBS; Gibco). RNA was extracted using Quick-RNA MiniPrepKit (Zymo Research) according to the manufacturers protocol. RNA (500 ng) was then converted to cDNA using the High-Capacity Reverse Transcription Kit (Applied Biosystems). qPCR reactions were prepared using Power SYBR Green PCR Master Mix (Applied Biosystems), and primers (below) were obtained from Integrated DNA Technologies. Amplification reactions were run in an ABI 7900HT Fast Real Time PCR machine with an initial melting period of 95 °C for 5 min and then 45 cycles of 10 s at 95 °C, 30 s at 60 °C.

qPCR Primers

	Forward	Reverse
<i>M. musculus Chac1</i>	TGACCCCTCCTTGAAGACCGTGA	AGTGTCA TAGCCACCAAGCACG
<i>M. musculus RiboP</i>	TGTCATCGCTCAGGGTGTG	AAGCCAATCCCATGTCGTC
<i>M. musculus Asns</i>	CCAAGTTCA GTATCCTCTCC	TAATTGCCACCTTCTAGC
<i>H. sapiens 36b4</i>	CCACGCTGCTGAACATGC	TCGAACACCTGCTGGATGAC
<i>H. sapiens ASNS</i>	ATCACTGTCGGGATGTACCC	TGATAAAAGGCAGCCAATCC
<i>H. sapiens CHAC1</i>	GTGGTGACGCTCCTTGAAGA	TTCAGGGCCTTGCTTACCTG
<i>H. sapiens HSPA1A</i>	GCTGATGATGGGGTTAAC	GGAGGCAGGAGTACA

H. sapiens NQO1

GCCTCCTTCATGGCATAGTT

GGACTGCACCAGAGCCAT

Fluorescence Microscopy

MEF^{mtGFP} were seeded at a density of 15,000 cells/well in 8-chamber slides (Ibidi) coated with poly-D-lysine (Sigma).⁵⁸ The next day cells were treated with the indicated dose of compound for the indicated time. After treatment, cells were imaged on a Zeiss LSM 880 Confocal Laser Scanning Microscope equipped with a full incubation chamber for regulating temperature and CO₂ during live cell imaging.

Patient fibroblasts were seeded at 70,000 cells per dish in 35 mm dishes with 20mm glass bottoms (D35-20-1.5-N, Cellvis) for live-cell imaging. After 24 hours, the compound treatments were administered at the dosage and for the time points indicated in the figure legends. The mitochondrial network in patient fibroblasts was visualized using 100 nM MitoTracker Green (M7514, Life Technologies)⁸³ for 45 minutes, following washing three times with culture media, according to the manufacturer's instructions. The Z-stack images were acquired of patient fibroblasts using an Olympus Spinning Disc Confocal System (Olympus SD OSR) equipped with the Olympus UPlanApo 60XTIRF/1.50 Oil Objective using the CellSense Dimensions software. Acquired Z-stacks were analyzed using AI Machine Learning Segmentation (Imaris), as detailed below.

Quantification of mitochondrial morphology.

The z-stack confocal images were processed in FIJI to reduce the background noise and enhance the fluorescent signal. The processed images are then introduced into the developed quantification pipeline in Imaris imaging software. In this approach, mitochondria are segmented in 3D using the “Surfaces” module with a machine-learning algorithm that has been iteratively trained to detect foreground and background pixels in each z-stack, filling blank holes within segments to generate 3D surfaces. The generated surfaces are filtered to include those above a minimum threshold of 250 voxels. While direct length measurements cannot be obtained through the Imaris surface module, indirect measurements of mitochondrial length are inferred from three separate calculations, including (1) object-oriented bounding box axis, (2) ellipsoid axis length, and (3) object sphericity (see **Fig. S2A**). The object-oriented bounding box axis is calculated by measuring the length of the longest or principal bounding-box length of the smallest object-oriented rectangular box that encloses each 3D segmentation. The ellipsoid axis length is calculated by measuring the length of the longest or principal axis of

each 3D segmentation. Sphericity is calculated by dividing the longest axis of each 3D segmentation by the length of the perpendicular axis.

Statistical Methods.

Data are presented as mean ± SEM or as violin plots showing the mean and quartiles for the indicated number of measurements. Outliers were removed from datasets describing bounding box length and principal axis length, as appropriate, using the ROUT outlier test in PRISM 10 (GraphPad, San Diego, CA). Normality of datasets from our imaging studies was tested in PRISM 10 (GraphPad, San Diego, CA) using D'Agostino & Pearson, Anderson-Darling, Shapiro-Wilk, and Kolmogorov-Smirnov tests. Statistics were calculated in PRISM 10 (GraphPad, San Diego, CA) and analyzed by one-way ANOVA with Tukey's multiple correction test, Kruskal-Wallis or Mann-Whitney tests for data exhibiting a non-normal distribution, as indicated in the accompanying figure legends. Indications of nonsignificant interactions were generally omitted for clarity.

ACKNOWLEDGEMENTS

We thank Prerona Bora, Jie Sun, and Sergei Kutseikin for experimental support and Evan Powers for critical reading of the manuscript. We thank Kathy Spencer and Scott Henderson in the TSRI Microscopy Facility for their support on the confocal imaging and analysis described in this project. We would also like to thank Martin Kampmann (UCSF), Xiaoyan Guo (UConn), and Jonathan Lin (Stanford) for experimental resources and advice related to this project. This work was supported by the National Institutes of Health (NIH; NS095892, NS125674 to RLW), the Canadian Institutes of Health Research (TES), an NIH F30 Predoctoral Fellowship (AG081061 to KB), National Science Foundation Predoctoral Fellowships (to SO and RA), and the Hotchkiss Brain Institute International Recruitment Scholarship (MZ).

CONFLICT OF INTEREST STATEMENT

The authors declare no conflict of interest for the work presented in this manuscript.

REFERENCES

- 1 Costa-Mattioli, M. & Walter, P. The integrated stress response: From mechanism to disease. *Science* **368**, doi:10.1126/science.aat5314 (2020).

- 2 Pakos-Zebrucka, K., Koryga, I., Mnich, K., Ljubic, M., Samali, A. & Gorman, A. M. The integrated stress response. *EMBO Rep* **17**, 1374-1395, doi:10.15252/embr.201642195 (2016).
- 3 Anderson, N. S. & Haynes, C. M. Folding the Mitochondrial UPR into the Integrated Stress Response. *Trends Cell Biol* **30**, 428-439, doi:10.1016/j.tcb.2020.03.001 (2020).
- 4 Quiros, P. M., Mottis, A. & Auwerx, J. Mitonuclear communication in homeostasis and stress. *Nat Rev Mol Cell Biol* **17**, 213-226, doi:10.1038/nrm.2016.23 (2016).
- 5 Winter, J. M., Yadav, T. & Rutter, J. Stressed to death: Mitochondrial stress responses connect respiration and apoptosis in cancer. *Mol Cell* **82**, 3321-3332, doi:10.1016/j.molcel.2022.07.012 (2022).
- 6 Fessler, E., Eckl, E. M., Schmitt, S., Mancilla, I. A., Meyer-Bender, M. F., Hanf, M., Philippou-Massier, J., Krebs, S., Zischka, H. & Jae, L. T. A pathway coordinated by DELE1 relays mitochondrial stress to the cytosol. *Nature* **579**, 433-437, doi:10.1038/s41586-020-2076-4 (2020).
- 7 Fessler, E., Krumwiede, L. & Jae, L. T. DELE1 tracks perturbed protein import and processing in human mitochondria. *Nat Commun* **13**, 1853, doi:10.1038/s41467-022-29479-y (2022).
- 8 Guo, X., Aviles, G., Liu, Y., Tian, R., Unger, B. A., Lin, Y. T., Wiita, A. P., Xu, K., Correia, M. A. & Kampmann, M. Mitochondrial stress is relayed to the cytosol by an OMA1-DELE1-HRI pathway. *Nature* **579**, 427-432, doi:10.1038/s41586-020-2078-2 (2020).
- 9 Sekine, Y., Houston, R., Eckl, E. M., Fessler, E., Narendra, D. P., Jae, L. T. & Sekine, S. A mitochondrial iron-responsive pathway regulated by DELE1. *Mol Cell* **83**, 2059-2076 e2056, doi:10.1016/j.molcel.2023.05.031 (2023).
- 10 Yang, J., Baron, K. R., Pride, D. E., Schneemann, A., Guo, X., Chen, W., Song, A. S., Aviles, G., Kampmann, M., Wiseman, R. L. & Lander, G. C. DELE1 oligomerization promotes integrated stress response activation. *Nat Struct Mol Biol* **30**, 1295-1302, doi:10.1038/s41594-023-01061-0 (2023).
- 11 Yang, J., Baron, K. R., Pride, D. E., Schneemann, A., Guo, X., Chen, W., Song, A. S., Aviles, G., Kampmann, M., Luke Wiseman, R. & Lander, G. C. DELE1 oligomerization promotes integrated stress response activation. *Nat Struct Mol Biol* **30**, 1295-1302, doi:10.1038/s41594-023-01061-0 (2023).
- 12 Mick, E., Titov, D. V., Skinner, O. S., Sharma, R., Jourdain, A. A. & Mootha, V. K. Distinct mitochondrial defects trigger the integrated stress response depending on the metabolic state of the cell. *eLife* **9**, doi:10.7554/eLife.49178 (2020).
- 13 Madrazo, N., Khattar, Z., Powers, E. T., Rosarda, J. D. & Wiseman, R. L. Mapping Stress-Responsive Signaling Pathways Induced by Mitochondrial Proteostasis Perturbations. *Mol Biol Cell*, mbcE24010041, doi:10.1091/mbc.E24-01-0041 (2024).
- 14 Hori, O., Ichinoda, F., Tamatani, T., Yamaguchi, A., Sato, N., Ozawa, K., Kitao, Y., Miyazaki, M., Harding, H. P., Ron, D., Tohyama, M., D, M. S. & Ogawa, S. Transmission of cell stress from endoplasmic reticulum to mitochondria: enhanced expression of Lon protease. *J Cell Biol* **157**, 1151-1160, doi:10.1083/jcb.200108103 (2002).
- 15 Han, J., Back, S. H., Hur, J., Lin, Y. H., Gildersleeve, R., Shan, J., Yuan, C. L., Krokowski, D., Wang, S., Hatzoglou, M., Kilberg, M. S., Sartor, M. A. & Kaufman, R. J. ER-stress-induced transcriptional regulation increases protein synthesis leading to cell death. *Nat Cell Biol* **15**, 481-490, doi:10.1038/ncb2738 (2013).
- 16 Rainbolt, T. K., Atanassova, N., Genereux, J. C. & Wiseman, R. L. Stress-regulated translational attenuation adapts mitochondrial protein import through Tim17A degradation. *Cell Metab* **18**, 908-919, doi:10.1016/j.cmet.2013.11.006 (2013).
- 17 Balsa, E., Soustek, M. S., Thomas, A., Cogliati, S., Garcia-Poyatos, C., Martin-Garcia, E., Jedrychowski, M., Gygi, S. P., Enriquez, J. A. & Puigserver, P. ER and Nutrient Stress Promote Assembly of Respiratory Chain Supercomplexes through the PERK-eIF2alpha Axis. *Mol Cell* **74**, 877-890 e876, doi:10.1016/j.molcel.2019.03.031 (2019).
- 18 Barad, B. A., Medina, M., Fuentes, D., Wiseman, R. L. & Grotjahn, D. A. Quantifying organellar ultrastructure in cryo-electron tomography using a surface morphometrics pipeline. *J Cell Biol* **222**, doi:10.1083/jcb.202204093 (2023).
- 19 Latorre-Muro, P., O'Malley, K. E., Bennett, C. F., Perry, E. A., Balsa, E., Tavares, C. D. J., Jedrychowski, M., Gygi, S. P. & Puigserver, P. A cold-stress-inducible PERK/OGT axis controls TOM70-assisted mitochondrial protein import and cristae formation. *Cell Metab* **33**, 598-614 e597, doi:10.1016/j.cmet.2021.01.013 (2021).
- 20 Lebeau, J., Saunders, J. M., Moraes, V. W. R., Madhavan, A., Madrazo, N., Anthony, M. C. & Wiseman, R. L. The PERK Arm of the Unfolded Protein Response Regulates Mitochondrial Morphology during Acute Endoplasmic Reticulum Stress. *Cell Rep* **22**, 2827-2836, doi:10.1016/j.celrep.2018.02.055 (2018).

- 21 Perea, V., Cole, C., Lebeau, J., Dolina, V., Baron, K. R., Madhavan, A., Kelly, J. W., Grotjahn, D. A. & Wiseman, R. L. PERK signaling promotes mitochondrial elongation by remodeling membrane phosphatidic acid. *EMBO J* **42**, e113908, doi:10.15252/embj.2023113908 (2023).
- 22 Chan, D. C. Mitochondrial Dynamics and Its Involvement in Disease. *Annu Rev Pathol* **15**, 235-259, doi:10.1146/annurev-pathmechdis-012419-032711 (2020).
- 23 Quintana-Cabrera, R. & Scorrano, L. Determinants and outcomes of mitochondrial dynamics. *Mol Cell* **83**, 857-876, doi:10.1016/j.molcel.2023.02.012 (2023).
- 24 Perea, V., Baron, K. R., Dolina, V., Aviles, G., Kim, G., Rosarda, J. D., Guo, X., Kampmann, M. & Wiseman, R. L. Pharmacologic activation of a compensatory integrated stress response kinase promotes mitochondrial remodeling in PERK-deficient cells. *Cell Chem Biol*, doi:10.1016/j.chembiol.2023.10.006 (2023).
- 25 Sharma, G., Pfeffer, G. & Shutt, T. E. Genetic Neuropathy Due to Impairments in Mitochondrial Dynamics. *Biology (Basel)* **10**, doi:10.3390/biology10040268 (2021).
- 26 Chen, W., Zhao, H. & Li, Y. Mitochondrial dynamics in health and disease: mechanisms and potential targets. *Signal Transduct Target Ther* **8**, 333, doi:10.1038/s41392-023-01547-9 (2023).
- 27 Liu, Y. J., McIntyre, R. L., Janssens, G. E. & Houtkooper, R. H. Mitochondrial fission and fusion: A dynamic role in aging and potential target for age-related disease. *Mech Ageing Dev* **186**, 111212, doi:10.1016/j.mad.2020.111212 (2020).
- 28 Sprenger, H. G. & Langer, T. The Good and the Bad of Mitochondrial Breakups. *Trends Cell Biol* **29**, 888-900, doi:10.1016/j.tcb.2019.08.003 (2019).
- 29 Giacomello, M., Pyakurel, A., Glytsou, C. & Scorrano, L. The cell biology of mitochondrial membrane dynamics. *Nat Rev Mol Cell Biol* **21**, 204-224, doi:10.1038/s41580-020-0210-7 (2020).
- 30 Wai, T. & Langer, T. Mitochondrial Dynamics and Metabolic Regulation. *Trends Endocrinol Metab* **27**, 105-117, doi:10.1016/j.tem.2015.12.001 (2016).
- 31 Whitley, B. N., Engelhart, E. A. & Hoppins, S. Mitochondrial dynamics and their potential as a therapeutic target. *Mitochondrion* **49**, 269-283, doi:10.1016/j.mito.2019.06.002 (2019).
- 32 Bhatti, J. S., Kaur, S., Mishra, J., Dibbanti, H., Singh, A., Reddy, A. P., Bhatti, G. K. & Reddy, P. H. Targeting dynamin-related protein-1 as a potential therapeutic approach for mitochondrial dysfunction in Alzheimer's disease. *Biochim Biophys Acta Mol Basis Dis* **1869**, 166798, doi:10.1016/j.bbadi.2023.166798 (2023).
- 33 Gu, Y., Guerra, F., Hu, M., Pope, A., Sung, K., Yang, W., Jetha, S., Shoff, T. A., Gunatilake, T., Dahlkamp, O., Shi, L. Z., Manganelli, F., Nolano, M., Zhou, Y., Ding, J., Bucci, C. & Wu, C. Mitochondria dysfunction in Charcot Marie Tooth 2B Peripheral Sensory Neuropathy. *Commun Biol* **5**, 717, doi:10.1038/s42003-022-03632-1 (2022).
- 34 Das, R., Kamal, I. M., Das, S., Chakrabarti, S. & Chakrabarti, O. MITOL-mediated DRP1 ubiquitylation and degradation promotes mitochondrial hyperfusion in a CMT2A-linked MFN2 mutant. *J Cell Sci* **135**, doi:10.1242/jcs.257808 (2022).
- 35 Chen, Z., Chai, E., Mou, Y., Roda, R. H., Blackstone, C. & Li, X. J. Inhibiting mitochondrial fission rescues degeneration in hereditary spastic paraplegia neurons. *Brain* **145**, 4016-4031, doi:10.1093/brain/awab488 (2022).
- 36 Yang, J., Chen, P., Cao, Y., Liu, S., Wang, W., Li, L., Li, J., Jiang, Z., Ma, Y., Chen, S., Zheng, S., Qi, X. & Jiang, H. Chemical inhibition of mitochondrial fission via targeting the DRP1-receptor interaction. *Cell Chem Biol* **30**, 278-294 e211, doi:10.1016/j.chembiol.2023.02.002 (2023).
- 37 Guo, X., Disatnik, M. H., Monbureau, M., Shamloo, M., Mochly-Rosen, D. & Qi, X. Inhibition of mitochondrial fragmentation diminishes Huntington's disease-associated neurodegeneration. *J Clin Invest* **123**, 5371-5388, doi:10.1172/JCI70911 (2013).
- 38 Joshi, A. U., Saw, N. L., Vogel, H., Cunningham, A. D., Shamloo, M. & Mochly-Rosen, D. Inhibition of Drp1/Fis1 interaction slows progression of amyotrophic lateral sclerosis. *EMBO Mol Med* **10**, doi:10.15252/emmm.201708166 (2018).
- 39 Bera, A., Lavanya, G., Reshma, R., Dev, K. & Kumar, R. Mechanistic and therapeutic role of Drp1 in the pathogenesis of Alzheimer's disease. *Eur J Neurosci* **56**, 5516-5531, doi:10.1111/ejn.15611 (2022).
- 40 Manczak, M., Kandimalla, R., Fry, D., Sesaki, H. & Reddy, P. H. Protective effects of reduced dynamin-related protein 1 against amyloid beta-induced mitochondrial dysfunction and synaptic damage in Alzheimer's disease. *Hum Mol Genet* **25**, 5148-5166, doi:10.1093/hmg/ddw330 (2016).
- 41 Kandimalla, R., Manczak, M., Pradeepkiran, J. A., Morton, H. & Reddy, P. H. A partial reduction of Drp1 improves cognitive behavior and enhances mitophagy, autophagy and dendritic spines in a transgenic

- Tau mouse model of Alzheimer disease. *Hum Mol Genet* **31**, 1788-1805, doi:10.1093/hmg/ddab360 (2022).
- 42 Yan, J., Liu, X. H., Han, M. Z., Wang, Y. M., Sun, X. L., Yu, N., Li, T., Su, B. & Chen, Z. Y. Blockage of GSK3beta-mediated Drp1 phosphorylation provides neuroprotection in neuronal and mouse models of Alzheimer's disease. *Neurobiol Aging* **36**, 211-227, doi:10.1016/j.neurobiolaging.2014.08.005 (2015).
- 43 Baek, S. H., Park, S. J., Jeong, J. I., Kim, S. H., Han, J., Kyung, J. W., Baik, S. H., Choi, Y., Choi, B. Y., Park, J. S., Bahn, G., Shin, J. H., Jo, D. S., Lee, J. Y., Jang, C. G., Arumugam, T. V., Kim, J., Han, J. W., Koh, J. Y., Cho, D. H. & Jo, D. G. Inhibition of Drp1 Ameliorates Synaptic Depression, Abeta Deposition, and Cognitive Impairment in an Alzheimer's Disease Model. *J Neurosci* **37**, 5099-5110, doi:10.1523/JNEUROSCI.2385-16.2017 (2017).
- 44 Mou, Y. & Li, X. J. Rescue axonal defects by targeting mitochondrial dynamics in hereditary spastic paraplegias. *Neural Regen Res* **14**, 574-577, doi:10.4103/1673-5374.248108 (2019).
- 45 Keller, T. L., Zocco, D., Sundrud, M. S., Hendrick, M., Edenuis, M., Yum, J., Kim, Y. J., Lee, H. K., Cortese, J. F., Wirth, D. F., Dignam, J. D., Rao, A., Yeo, C. Y., Mazitschek, R. & Whitman, M. Halofuginone and other febrifugine derivatives inhibit prolyl-tRNA synthetase. *Nat Chem Biol* **8**, 311-317, doi:10.1038/nchembio.790 (2012).
- 46 Perea, V., Baron, K. R., Dolina, V., Aviles, G., Kim, G., Rosarda, J. D., Guo, X., Kampmann, M. & Wiseman, R. L. Pharmacologic activation of a compensatory integrated stress response kinase promotes mitochondrial remodeling in PERK-deficient cells. *Cell Chem Biol* **30**, 1571-1584 e1575, doi:10.1016/j.chembiol.2023.10.006 (2023).
- 47 Ji, W. K., Hatch, A. L., Merrill, R. A., Strack, S. & Higgs, H. N. Actin filaments target the oligomeric maturation of the dynamin GTPase Drp1 to mitochondrial fission sites. *eLife* **4**, e11553, doi:10.7554/eLife.11553 (2015).
- 48 Ji, W. K., Chakrabarti, R., Fan, X., Schoenfeld, L., Strack, S. & Higgs, H. N. Receptor-mediated Drp1 oligomerization on endoplasmic reticulum. *J Cell Biol* **216**, 4123-4139, doi:10.1083/jcb.201610057 (2017).
- 49 Sharma, G., Zaman, M., Sabouny, R., Joel, M., Martens, K., Martino, D., de Koning, A. P. J., Pfeffer, G. & Shutt, T. E. Characterization of a novel variant in the HR1 domain of MFN2 in a patient with ataxia, optic atrophy and sensorineural hearing loss. *F1000Res* **10**, 606, doi:10.12688/f1000research.53230.2 (2021).
- 50 Sidrauski, C., Acosta-Alvear, D., Khoutorsky, A., Vedantham, P., Hearn, B. R., Li, H., Gamache, K., Gallagher, C. M., Ang, K. K., Wilson, C., Okreglak, V., Ashkenazi, A., Hann, B., Nader, K., Arkin, M. R., Renslo, A. R., Sonenberg, N. & Walter, P. Pharmacological brake-release of mRNA translation enhances cognitive memory. *eLife* **2**, e00498, doi:10.7554/eLife.00498 (2013).
- 51 Zyryanova, A. F., Weis, F., Faille, A., Alard, A. A., Crespillo-Casado, A., Sekine, Y., Harding, H. P., Allen, F., Parts, L., Fromont, C., Fischer, P. M., Warren, A. J. & Ron, D. Binding of ISRIB reveals a regulatory site in the nucleotide exchange factor eIF2B. *Science* **359**, 1533-1536, doi:10.1126/science.aar5129 (2018).
- 52 Kress, J. K. C., Jessen, C., Hufnagel, A., Schmitz, W., Xavier da Silva, T. N., Ferreira Dos Santos, A., Mosteo, L., Goding, C. R., Friedmann Angeli, J. P. & Meierjohann, S. The integrated stress response effector ATF4 is an obligatory metabolic activator of NRF2. *Cell Rep* **42**, 112724, doi:10.1016/j.celrep.2023.112724 (2023).
- 53 Grandjean, J. M. D., Plate, L., Morimoto, R. I., Bollong, M. J., Powers, E. T. & Wiseman, R. L. Deconvoluting Stress-Responsive Proteostasis Signaling Pathways for Pharmacologic Activation Using Targeted RNA Sequencing. *ACS Chem Biol* **14**, 784-795, doi:10.1021/acschembio.9b00134 (2019).
- 54 Grandjean, J. M. D., Madhavan, A., Cech, L., Seguinot, B. O., Paxman, R. J., Smith, E., Scampavia, L., Powers, E. T., Cooley, C. B., Plate, L., Spicer, T. P., Kelly, J. W. & Wiseman, R. L. Pharmacologic IRE1/XBP1s activation confers targeted ER proteostasis reprogramming. *Nat Chem Biol* **16**, 1052-1061, doi:10.1038/s41589-020-0584-z (2020).
- 55 Plate, L., Cooley, C. B., Chen, J. J., Paxman, R. J., Gallagher, C. M., Madoux, F., Genereux, J. C., Dobbs, W., Garza, D., Spicer, T. P., Scampavia, L., Brown, S. J., Rosen, H., Powers, E. T., Walter, P., Hodder, P., Wiseman, R. L. & Kelly, J. W. Small molecule proteostasis regulators that reprogram the ER to reduce extracellular protein aggregation. *eLife* **5**, doi:10.7554/eLife.15550 (2016).
- 56 Calamini, B., Silva, M. C., Madoux, F., Hutt, D. M., Khanna, S., Chalfant, M. A., Saldanha, S. A., Hodder, P., Tait, B. D., Garza, D., Balch, W. E. & Morimoto, R. I. Small-molecule proteostasis regulators for protein conformational diseases. *Nat Chem Biol* **8**, 185-196, doi:10.1038/nchembio.763 (2011).

- 57 Ibrahim, L., Mesgarzadeh, J., Xu, I., Powers, E. T., Wiseman, R. L. & Bollong, M. J. Defining the Functional Targets of Cap'n'collar Transcription Factors NRF1, NRF2, and NRF3. *Antioxidants (Basel)* **9**, doi:10.3390/antiox9101025 (2020).
- 58 Wang, D., Wang, J., Bonamy, G. M., Meeusen, S., Brusch, R. G., Turk, C., Yang, P. & Schultz, P. G. A small molecule promotes mitochondrial fusion in mammalian cells. *Angew Chem Int Ed Engl* **51**, 9302-9305, doi:10.1002/anie.201204589 (2012).
- 59 Calvo-Rodriguez, M. & Bacskai, B. J. High mitochondrial calcium levels precede neuronal death in vivo in Alzheimer's disease. *Cell Stress* **4**, 187-190, doi:10.15698/cst2020.07.226 (2020).
- 60 Calvo-Rodriguez, M., Hou, S. S., Snyder, A. C., Kharitonova, E. K., Russ, A. N., Das, S., Fan, Z., Muzikansky, A., Garcia-Alloza, M., Serrano-Pozo, A., Hudry, E. & Bacskai, B. J. Increased mitochondrial calcium levels associated with neuronal death in a mouse model of Alzheimer's disease. *Nat Commun* **11**, 2146, doi:10.1038/s41467-020-16074-2 (2020).
- 61 Garbincius, J. F. & Elrod, J. W. Mitochondrial calcium exchange in physiology and disease. *Physiol Rev* **102**, 893-992, doi:10.1152/physrev.00041.2020 (2022).
- 62 Matuz-Mares, D., Gonzalez-Andrade, M., Araiza-Villanueva, M. G., Vilchis-Landeros, M. M. & Vazquez-Meza, H. Mitochondrial Calcium: Effects of Its Imbalance in Disease. *Antioxidants (Basel)* **11**, doi:10.3390/antiox11050801 (2022).
- 63 Cartoni, R. & Martinou, J. C. Role of mitofusin 2 mutations in the physiopathology of Charcot-Marie-Tooth disease type 2A. *Exp Neurol* **218**, 268-273, doi:10.1016/j.expneurol.2009.05.003 (2009).
- 64 Zaman, M. & Shutt, T. E. The Role of Impaired Mitochondrial Dynamics in MFN2-Mediated Pathology. *Front Cell Dev Biol* **10**, 858286, doi:10.3389/fcell.2022.858286 (2022).
- 65 Alberti, C., Rizzo, F., Anastasia, A., Comi, G., Corti, S. & Abati, E. Charcot-Marie-tooth disease type 2A: An update on pathogenesis and therapeutic perspectives. *Neurobiol Dis* **193**, 106467, doi:10.1016/j.nbd.2024.106467 (2024).
- 66 Yu, T., Wang, L., Zhang, L. & Deuster, P. A. Mitochondrial Fission as a Therapeutic Target for Metabolic Diseases: Insights into Antioxidant Strategies. *Antioxidants (Basel)* **12**, doi:10.3390/antiox12061163 (2023).
- 67 Gorman, G. S., Chinnery, P. F., DiMauro, S., Hirano, M., Koga, Y., McFarland, R., Suomalainen, A., Thorburn, D. R., Zeviani, M. & Turnbull, D. M. Mitochondrial diseases. *Nat Rev Dis Primers* **2**, 16080, doi:10.1038/nrdp.2016.80 (2016).
- 68 Lightowers, R. N., Taylor, R. W. & Turnbull, D. M. Mutations causing mitochondrial disease: What is new and what challenges remain? *Science* **349**, 1494-1499, doi:10.1126/science.aac7516 (2015).
- 69 Song, J., Herrmann, J. M. & Becker, T. Quality control of the mitochondrial proteome. *Nat Rev Mol Cell Biol* **22**, 54-70, doi:10.1038/s41580-020-00300-2 (2021).
- 70 Deshwal, S., Fiedler, K. U. & Langer, T. Mitochondrial Proteases: Multifaceted Regulators of Mitochondrial Plasticity. *Annu Rev Biochem* **89**, 501-528, doi:10.1146/annurev-biochem-062917-012739 (2020).
- 71 Yoshimura, A., Yuan, J. H., Hashiguchi, A., Ando, M., Higuchi, Y., Nakamura, T., Okamoto, Y., Nakagawa, M. & Takashima, H. Genetic profile and onset features of 1005 patients with Charcot-Marie-Tooth disease in Japan. *J Neurol Neurosurg Psychiatry* **90**, 195-202, doi:10.1136/jnnp-2018-318839 (2019).
- 72 Pisciotta, C., Saveri, P. & Pareyson, D. Updated review of therapeutic strategies for Charcot-Marie-Tooth disease and related neuropathies. *Expert Rev Neurother* **21**, 701-713, doi:10.1080/14737175.2021.1935242 (2021).
- 73 Park, G., Xu, K., Chea, L., Kim, K., Safarta, L., Song, K. H., Wu, J., Park, S., Min, H., Hiramatsu, N., Han, J. & Lin, J. H. Neurodegeneration risk factor, EIF2AK3 (PERK), influences tau protein aggregation. *J Biol Chem* **299**, 102821, doi:10.1016/j.jbc.2022.102821 (2023).
- 74 Yuan, S. H., Hiramatsu, N., Liu, Q., Sun, X. V., Lenh, D., Chan, P., Chiang, K., Koo, E. H., Kao, A. W., Litvan, I. & Lin, J. H. Tauopathy-associated PERK alleles are functional hypomorphs that increase neuronal vulnerability to ER stress. *Hum Mol Genet* **27**, 3951-3963, doi:10.1093/hmg/ddy297 (2018).
- 75 Ganz, J., Shacham, T., Kramer, M., Shenkman, M., Eiger, H., Weinberg, N., Iancovalici, O., Roy, S., Simhaev, L., Da'adoosh, B., Engel, H., Perets, N., Barhum, Y., Portnoy, M., Offen, D. & Ledermann, G. Z. A novel specific PERK activator reduces toxicity and extends survival in Huntington's disease models. *Sci Rep* **10**, 6875, doi:10.1038/s41598-020-63899-4 (2020).
- 76 Stockwell, S. R., Platt, G., Barrie, S. E., Zoumpoulidou, G., Te Poele, R. H., Aherne, G. W., Wilson, S. C., Sheldrake, P., McDonald, E., Venet, M., Soudy, C., Elustondo, F., Rigoreau, L., Blagg, J., Workman, P., Garrett, M. D. & Mittnacht, S. Mechanism-based screen for G1/S checkpoint activators identifies a

- selective activator of EIF2AK3/PERK signalling. *PLoS One* **7**, e28568, doi:10.1371/journal.pone.0028568 (2012).
- 77 Chen, T., Ozel, D., Qiao, Y., Harbinski, F., Chen, L., Denoyelle, S., He, X., Zvereva, N., Supko, J. G., Chorev, M., Halperin, J. A. & Aktas, B. H. Chemical genetics identify eIF2alpha kinase heme-regulated inhibitor as an anticancer target. *Nat Chem Biol* **7**, 610-616, doi:10.1038/nchembio.613 (2011).
- 78 Szaruga, M., Janssen, D. A., de Miguel, C., Hodgson, G., Fatala, A., Pitera, A. P., Andreeva, A. & Bertolotti, A. Activation of the integrated stress response by inhibitors of its kinases. *Nat Commun* **14**, 5535, doi:10.1038/s41467-023-40823-8 (2023).
- 79 Carlson, K. R., Georgiadis, M. M., Tameire, F., Staschke, K. A. & Wek, R. C. Activation of Gcn2 by small molecules designed to be inhibitors. *J Biol Chem* **299**, 104595, doi:10.1016/j.jbc.2023.104595 (2023).
- 80 Thomson, C. G., Aicher, T. D., Cheng, W., Du, H., Dudgeon, C., Li, A. H., Li, B., Lightcap, E., Luo, D., Mulvihill, M., Pan, P., Rahemtulla, B. F., Rigby, A. C., Sherborne, B., Sood, S., Surguladze, D., Talbot, E. P. A., Tameire, F., Taylor, S., Wang, Y., Wojnarowicz, P., Xiao, F. & Ramurthy, S. Discovery of HC-7366: An Orally Bioavailable and Efficacious GCN2 Kinase Activator. *J Med Chem* **67**, 5259-5271, doi:10.1021/acs.jmedchem.3c02384 (2024).
- 81 Madhavan, A., Kok, B. P., Rius, B., Grandjean, J. M. D., Alabi, A., Albert, V., Sukiasyan, A., Powers, E. T., Galmozzi, A., Saez, E. & Wiseman, R. L. Pharmacologic IRE1/XBP1s activation promotes systemic adaptive remodeling in obesity. *Nat Commun* **13**, 608, doi:10.1038/s41467-022-28271-2 (2022).
- 82 Martens, K., Leckie, J., Fok, D., Wells, R. A., Chhibber, S. & Pfeffer, G. Case Report: Calpainopathy Presenting After Bone Marrow Transplantation, With Studies of Donor Genetic Content in Various Tissue Types. *Front Neurol* **11**, 604547, doi:10.3389/fneur.2020.604547 (2020).
- 83 Kumar, S., Bharti, A., Mishra, N. C., Raina, D., Kharbanda, S., Saxena, S. & Kufe, D. Targeting of the c-Abl tyrosine kinase to mitochondria in the necrotic cell death response to oxidative stress. *J Biol Chem* **276**, 17281-17285, doi:10.1074/jbc.M101414200 (2001).

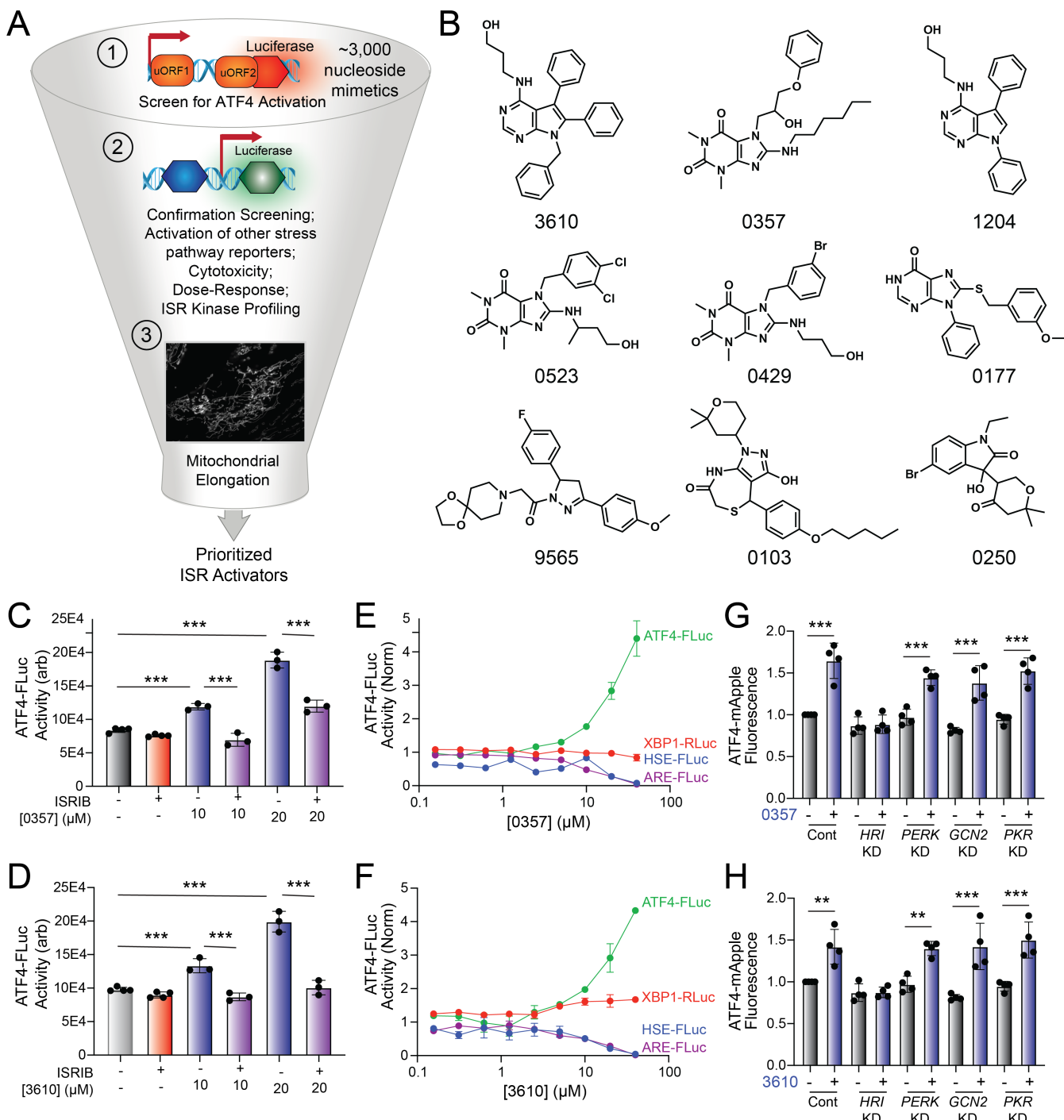


Figure 1. Identification of nucleoside mimetics that selectively activate the ISR kinase HRI. **A.** Screening pipeline used to identify selective ISR kinase activating compounds that promote protective mitochondrial elongation. **B.** Structures of the top 9 ISR activating compounds identified in our nucleoside mimetic screen. **C,D.** ATF4-FLuc activity in HEK293 cells stably expressing ATF4-FLuc¹¹ treated for 8 h with the indicated concentration of 0357 (**C**) or 3610 (**D**) in the absence or presence of ISRib (200 nM). **E,F.** Activation of the ATF4-FLuc ISR translational reporter (green), the XBP1-RLuc UPR reporter (red), the HSE-FLuc HSR reporter (blue) or the ARE-FLuc OSR reporter (purple) stably expressed in HEK293 cells treated with the indicated concentration of 0357 (**E**) or 3610 (**F**) for 16 h. **G,H.** ATF4-mAPPLE fluorescence in HEK293 cells stably expressing ATF4-mAPPLE and CRISPRi depleted of the indicated ISR kinase⁸ treated for 8 h with 0357 (**G**, 20 μM) or 3610 (**H**, 20 μM). **p<0.01, ***p<0.005 for one-way ANOVA.

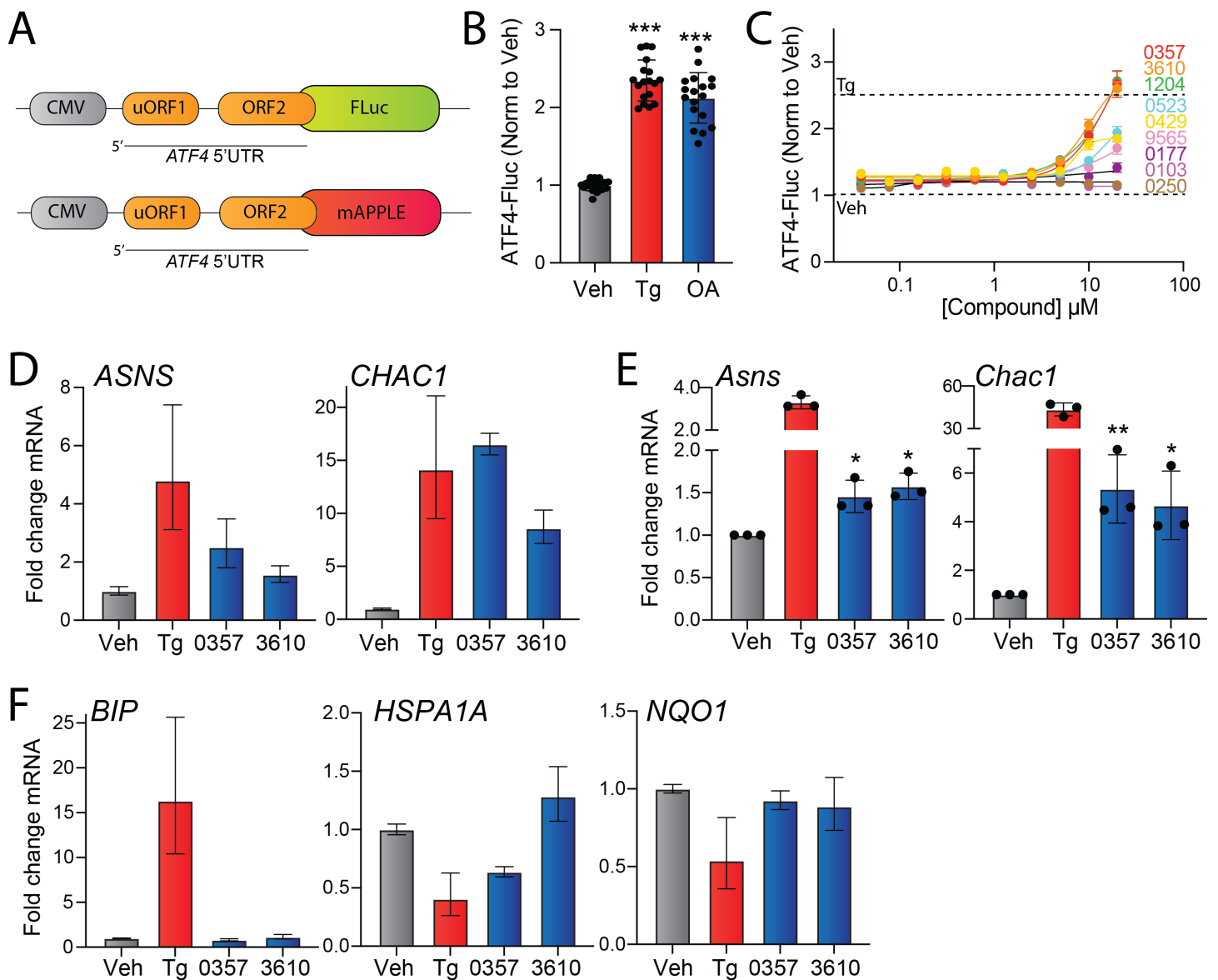


Figure S1 (Supplement to Figure 1). Identification of nucleoside mimetics that selectively activate the ISR kinase HRI. **A.** The ATF4-FLuc and ATF4-mAPPLE reporters containing the 5'UTR of ATF4.^{8,11} **B.** ATF4-GLuc activity, measured by luminescence, in HEK293 cells stably expressing ATF4-FLuc treated for 8 h with vehicle, thapsigargin (Tg, 0.5 μ M), or oligomycin A (OA, 50 ng/mL). **C.** ATF4-FLuc activity, normalized to vehicle, in HEK293 cells stably expressing ATF4-FLuc treated for 8 h with the indicated dose of the indicated compound. The signals observed in veh or thapsigargin (Tg, 0.5 μ M) cells is shown by the dashed lines. Error bars show SEM for n=9 replicates. **D.** Expression, measured by qPCR, of the ISR target genes ASNS and CHAC1 in HEK293 cells treated for 8 h with vehicle, thapsigargin (Tg; 0.5 μ M), 0357 (20 μ M), or 3610 (20 μ M). Error bars show 95% confidence intervals. **E.** Expression, measured by qPCR, of the ISR target genes Asns and Chac1 in MEF cells treated for 8 h with vehicle, thapsigargin (Tg; 0.5 μ M), 0357 (20 μ M), or 3610 (20 μ M). **F.** Expression, measured by qPCR, of the UPR target gene BiP, the HSR target gene HSPA1A, and the OSR target gene NQO1 in HEK293 cells treated for 8 h with vehicle, thapsigargin (Tg; 0.5 μ M), 0357 (20 μ M), or 3610 (20 μ M). Error bars show 95% confidence intervals. * $p<0.05$, *** $p<0.005$ for one-way ANOVA.

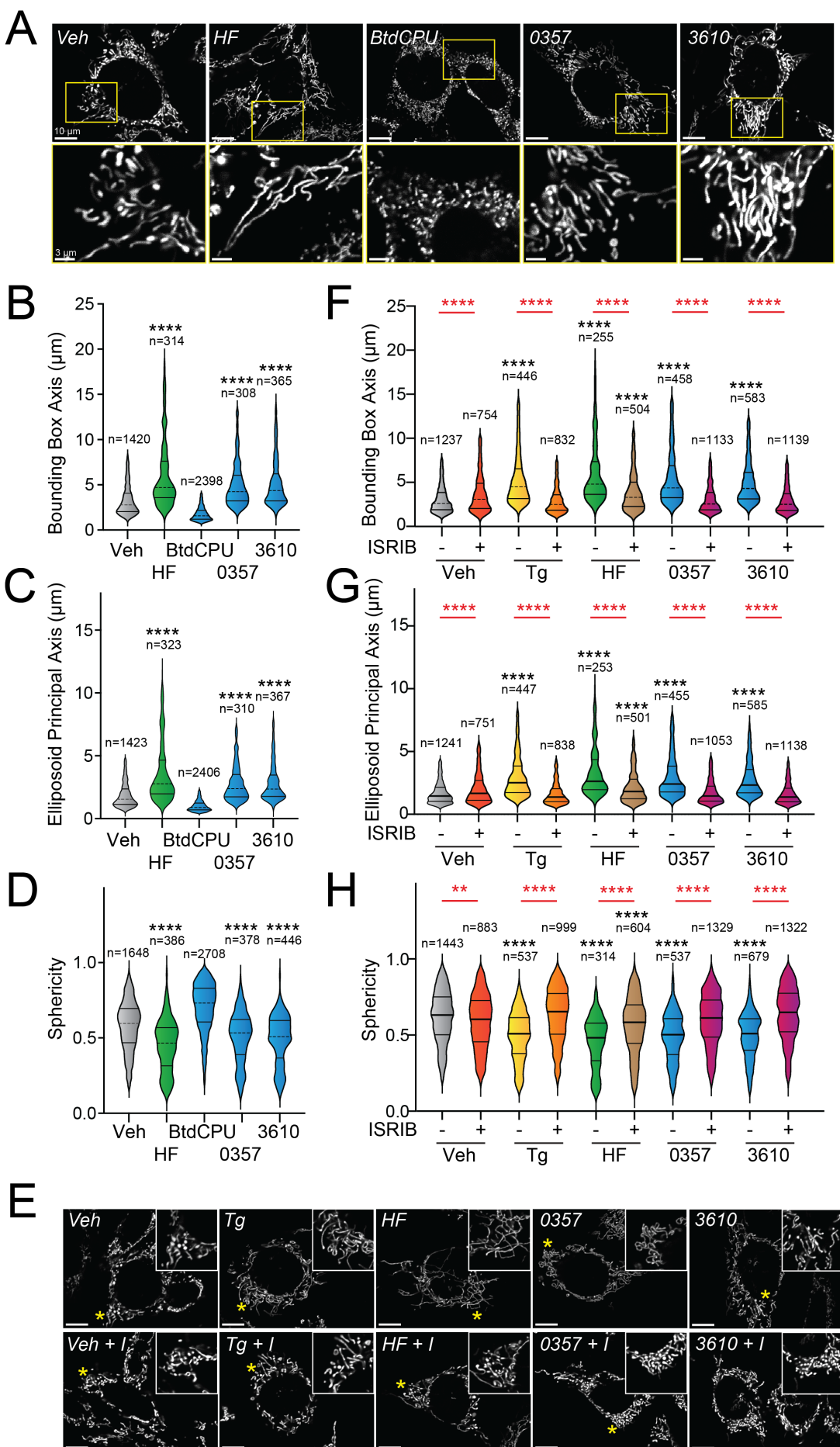
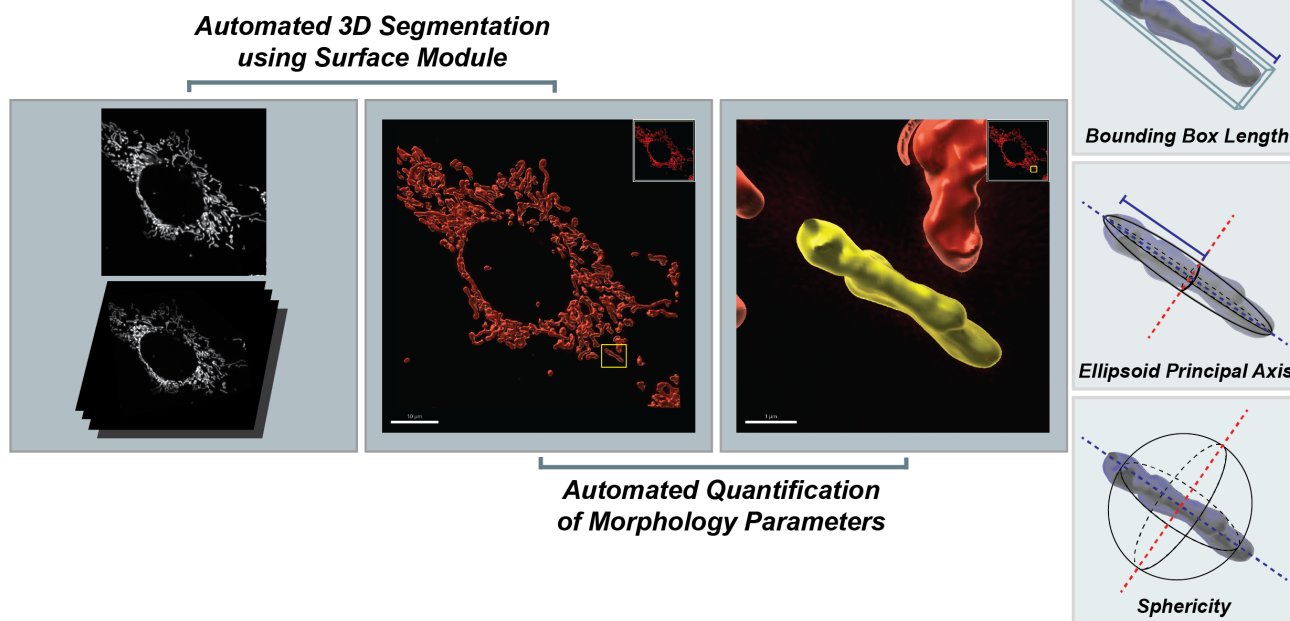
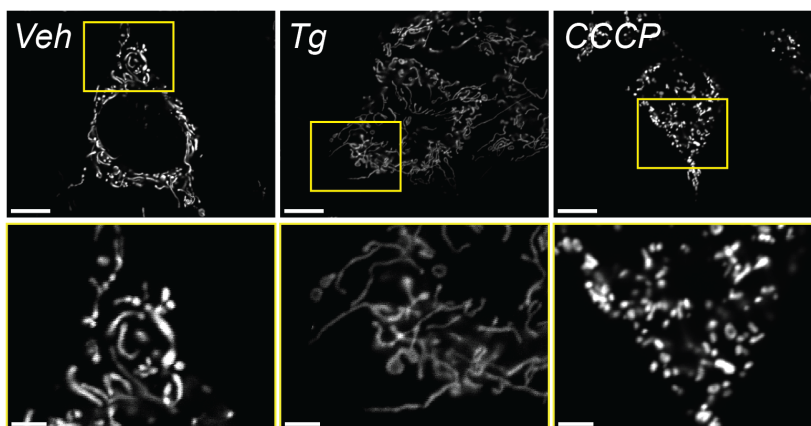


Figure 2. Pharmacologic HRI activation induces ISR-dependent mitochondrial elongation. A. Representative images of MEF cells stably expressing ^{mt}GFP (MEF^{mtGFP})⁵⁸ treated for 6 h with vehicle (veh), halofuginone (HF, 100 nM), BtdCPU (10 μ M), 0357 (10 μ M) or 3610 (10 μ M). The inset shows a 3-fold magnification of the region indicated by the yellow box. Scale bars, 10 μ m (top) and 3.33 μ m (bottom) **B-D.** Quantification of bounding box axis, ellipsoid principal axis, and sphericity from the entire dataset of representative images shown in **(A)**. The number of individual measurements for each condition are shown above. **E.** Representative images of MEF^{mtGFP} cells treated for 6 h with vehicle (veh), thapsigargin (Tg; 0.5 μ M) halofuginone (HF, 100 nM), 0357 (10 μ M) or 3610 (10 μ M) in the presence or absence of ISRIB (200 nM). The inset shows 3-fold magnification of the image centered on the asterisks. Scale bars, 10 μ m. **F-G.** Quantification of bounding box axis, ellipsoid principal axis, and sphericity from the entire dataset of representative images shown in **(E)**. The number of individual measurements for each condition are shown above. *p<0.05, ****p<0.001 for Kruskal-Wallis ANOVA. Black asterisks indicate comparison to vehicle treated cells. Red asterisks show comparisons for ISRIB co-treatment.

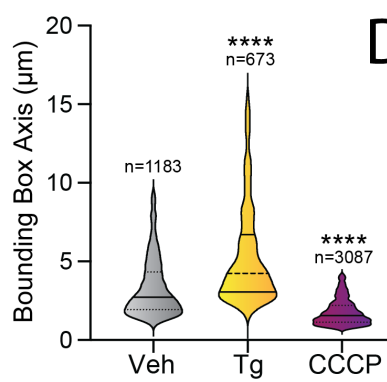
A



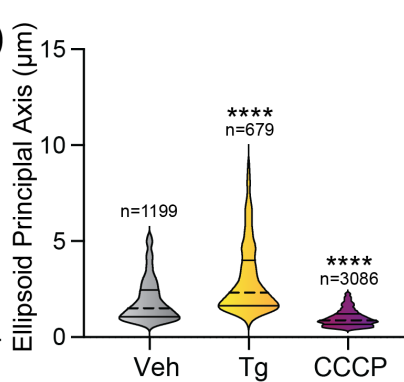
B



C



D



E

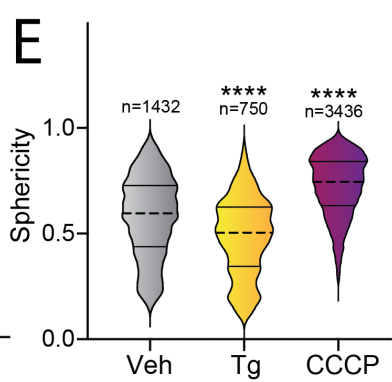


Figure S2 (Supplement Figure 2). Pharmacologic HRI activation induces ISR-dependent mitochondrial elongation. **A.** Image processing and analysis workflow to quantify several parameters that define mitochondrial shape. **B.** Representative images of MEF^{mtGFP} cells treated for 6 h with vehicle (veh), thapsigargin (Tg, 500 nM), or CCCP (10 μM). The inset shows a 3-fold magnification of the region indicated by the yellow box. Scale bars, 10 μm (top) and 3.33 μm (bottom) **C-E.** Quantification of bounding box axis, ellipsoid principal axis, and sphericity from the entire dataset of representative images shown in (B). The number of individual measurements for each condition are shown above. ***p<0.001 for Kruskal-Wallis ANOVA. Black asterisks show comparison with vehicle-treated cells.

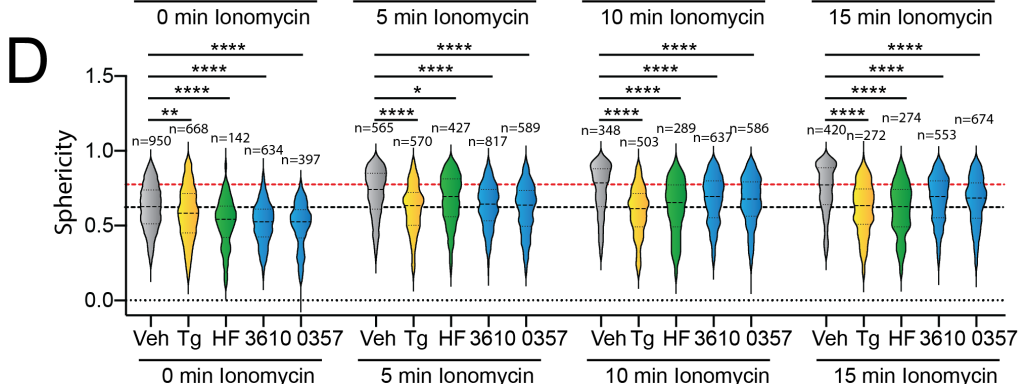
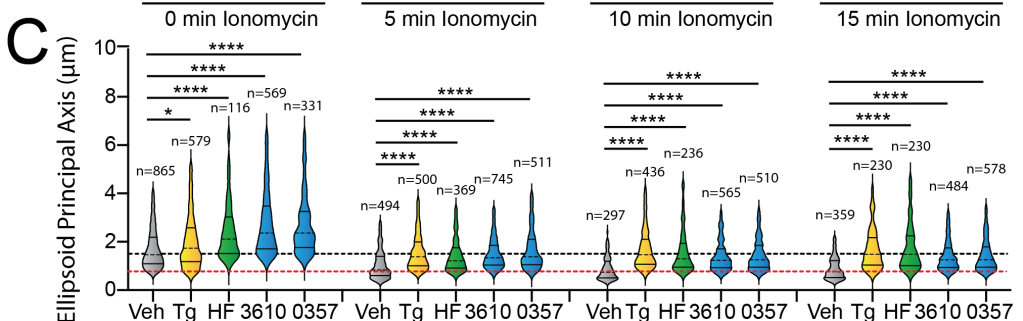
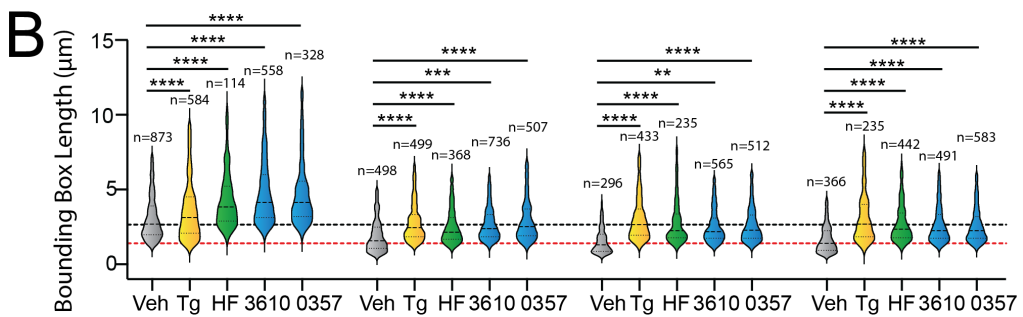
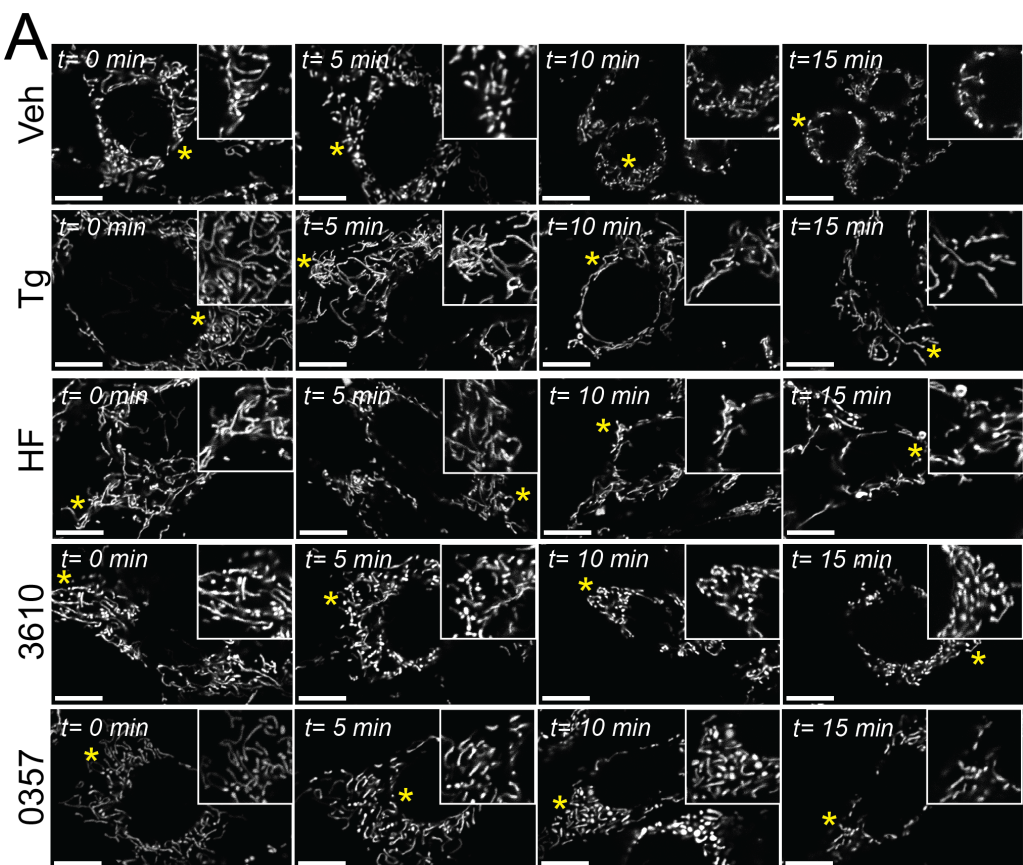


Figure 3. Stress-independent activation of ISR kinases prevents ionomycin-dependent accumulation of fragmented mitochondria. A. Representative images of MEF^{mtGFP} cells pre-treated for 6 h with vehicle (veh), thapsigargin (Tg, 500 nM), halofuginone (HF, 100 nM), 0357 (10 μ M) or 3610 (10 μ M) and then challenged with ionomycin (1 μ M) for the indicated time. The inset shows 3-fold magnification of the image centered on the asterisk. Scale bars, 10 μ m. **B-D.** Quantification of bounding box axis length, ellipsoid principal axis length, and sphericity from the entire dataset of representative images shown in **(A)**. The black dashed line shows the mean value of vehicle-treated cells prior to ionomycin treatment. The dashed red line shows the mean value of vehicle-treated cells following 15 min treatment with ionomycin. The number of individual measurements for each condition are shown above. * $p<0.05$, ** $p<0.01$, *** $p<0.005$, **** $p<0.001$ for Kruskal-Wallis ANOVA. Black asterisks show comparison with vehicle-treated cells.

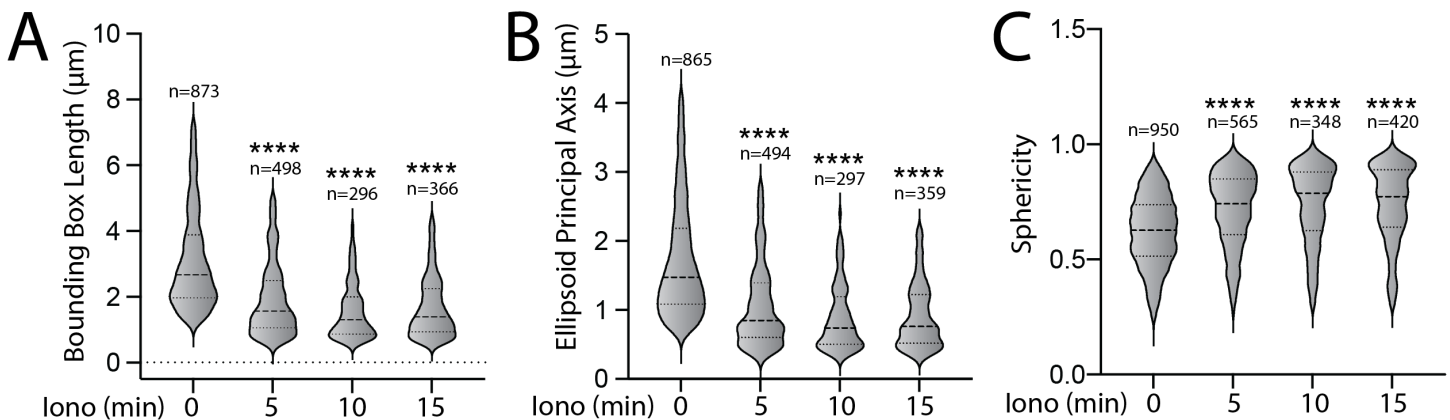


Figure S3. (Supplement to Figure 3). Stress-independent activation of ISR kinases prevents ionomycin-dependent accumulation of fragmented mitochondria. **A-C.** Quantifications of bounding box axis, ellipsoid principal axis, and sphericity of MEF^{mtGFP} cells pre-treated for 6 h with vehicle and then challenged with ionomycin (1 μM) for the indicated time. Representative images are shown in **Fig. 3A**. The number of individual measurements for each condition are shown above. ****p<0.001 for Kruskal-Wallis ANOVA. Black asterisks show comparison with vehicle-treated cells at time 0.

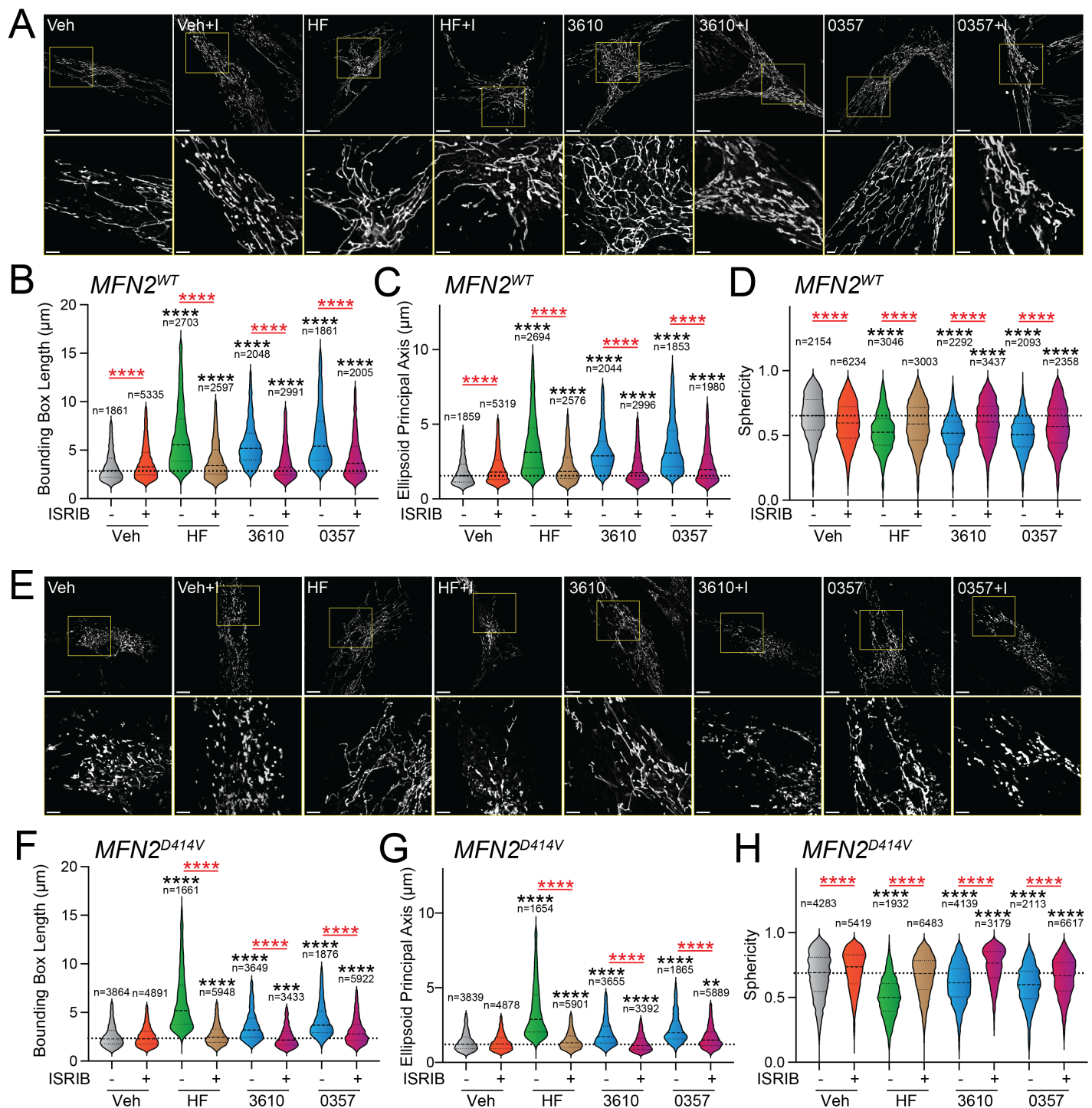


Figure 4. Pharmacologic activation of ISR kinases rescues basal mitochondrial morphology in patient fibroblasts expressing the disease-associated D414V MFN2 variant. A. Representative images of control human fibroblasts expressing *MFN2^{WT}* treated for 6 h with vehicle (veh), halofuginone (HF, 100 nM), 3610 (10 μM), 0357 (10 μM), and/or ISRIB (200 nM). The inset shows 3-fold magnification of the image centered on the asterisks. Scale bars, 15 μm (top) and 5 μM (bottom). **B-D.** Quantification of bounding box axis (**B**), ellipsoid principal axis (**C**), and sphericity (**D**) from the entire dataset of images described in panel **A**. The number of individual measurements for each condition are shown above. **E.** Representative images of patient fibroblasts expressing *MFN2^{D414V}* treated for 6 h with vehicle (veh), halofuginone (HF, 100 nM), 3610 (10 μM), 0357 (10 μM), and/or ISRIB (200 nM). The inset shows 3-fold magnification of the image centered on the asterisks. Scale bars, 15 μm (top) and 5 μM (bottom). **F-H.** Quantification of bounding box axis (**F**), ellipsoid principal axis (**G**), and sphericity (**H**) from the entire dataset of images described in panel **E**. The number of individual measurements for each condition are shown above. *p<0.05, **p<0.01, ***p<0.005, ****p<0.001 for Kruskal-Wallis ANOVA. Black asterisks show comparison with vehicle-treated cells. Red asterisks show comparisons for ISRIB co-treatment.

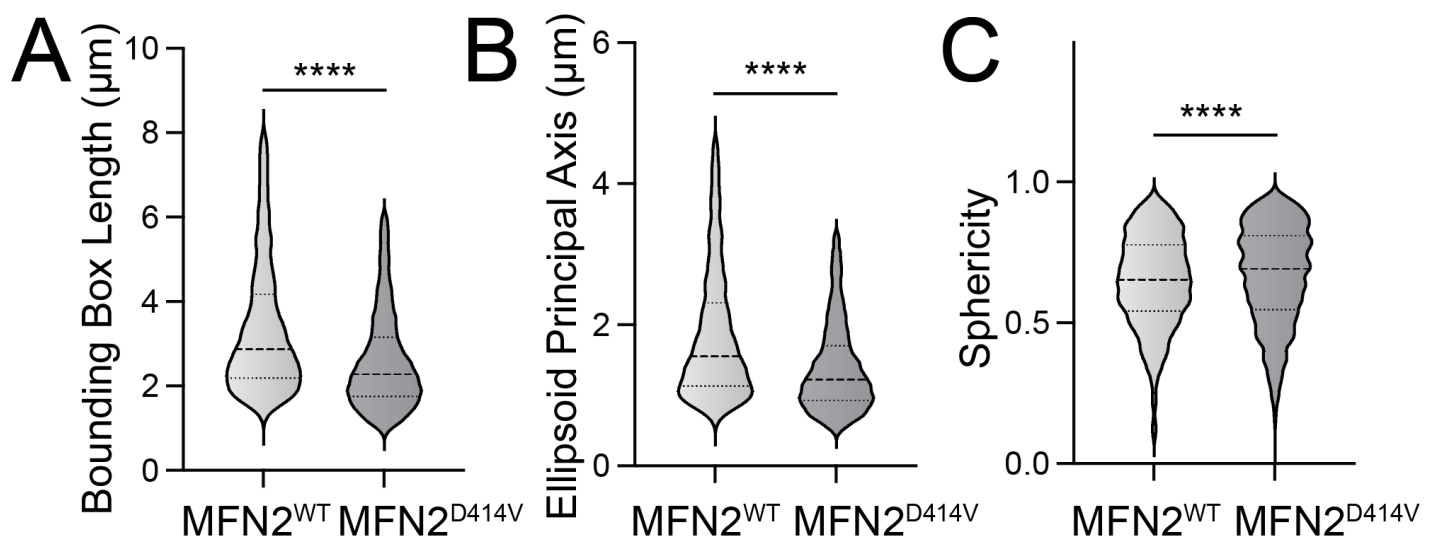


Figure S4 (Supplement to Figure 5). Pharmacologic activation of ISR kinases rescue basal mitochondrial morphology in patient fibroblasts expressing the disease-associated D414V MFN2 variant. A-C. Bounding box length (A), ellipsoid principal axis length (B), and sphericity (C) in control human fibroblasts expressing MFN2^{WT} or patient fibroblasts expressing MFN2^{D414V}. Representative images are shown in Fig. 4A,E. ***p<0.001 for Mann-Whitney t-test.